Engineering and Applied Science Letters

PSR Press

Article

Aged liver secreted factors lead to aging of human iPSC-derived heart muscle cells

Carly Lownes[1], Kimson Chitolie[1] and Aylin Acun[1,*]

[1] Biomedical Engineering Department, Widener University, Chester, PA 19013

* Correspondence: aacun@widener.edu

Received: 26 June 2025; Accepted: 28 August 2025; Published: 24 September 2025.

Abstract: Aging is a complex, systemic process often driven by both intrinsic and extrinsic factors. Recent evidence suggests that secretions from aging organs may influence the function of distant tissues. This study investigates the impact of liver-derived secretions from oxidatively aged cells on induced pluripotent stem cell-derived cardiomyocytes (iCMs). Here, we exposed HepG2 liver cells to hydrogen peroxide at varying concentrations (25–300 μM) and durations with regular intervals to model aging. Post-treatment validation confirmed increased oxidative stress, lipofuscin accumulation, p21 expression, and senescence, particularly in the 15-day 100 μM group. Conditioned media from aged HepG2 cultures were then applied to healthy, differentiated iCMs at various dilutions including undiluted, 1:1, and 1:3 with iCM media. iCMs exposed to aged liver secretions exhibited significantly increased aging phenotypes, including elevated lipofuscin and p21 expression, as well as increased senescent cell populations, with the strongest effects observed in undiluted and 1:1 treatment conditions. While senescence levels peaked at the 1:1 dilution rather than in undiluted media, a dose-dependent response to secreted stress factors was observed. Control experiments with untreated liver media showed no significant effects, confirming that the aging phenotypes observed in iCMs were driven specifically by the secretome of aged liver cells. These findings reveal a clear mechanism by which hepatic aging can promote cardiac aging and dysfunction, offering insight into liver-heart crosstalk in the context of human aging.

Keywords: aging, liver, heart, induced pluripotent stem cells, interorgan interactions

1. Introduction

Aging is a complex, irreversible biological process marked by the progressive decline of tissue function and regenerative capacity across organ systems, resulting in increased susceptibility to disease and death [1,2]. While intrinsic cellular mechanisms are known to drive many aspects of aging, accumulating evidence indicates that inter-organ communication (IOC) plays a critical role in systemic aging [3–6]. In particular, the liver, which plays a central role in metabolism, detoxification, and protein synthesis [7], may emerge as a key contributor to aging phenotypes in distant tissues through the secretion of bioactive molecules. With aging, the liver undergoes structural and functional changes, including increased extracellular matrix deposition, reduced regenerative capacity, and enhanced oxidative stress [8–11]. These changes are often accompanied by the release of altered secretory profiles, including pro-inflammatory cytokines, senescenceassociated secretory phenotype (SASP) factors, and extracellular vesicles (EVs) enriched with aging-related cargo [12–14].

Although the effects of these secreted factors on liver-resident cells have been explored, their potential impact on extrahepatic tissues, particularly the heart, remains inadequately understood. Cardiomyocytes are especially susceptible to oxidative and metabolic stress, and research suggests organ crosstalk may contribute to cardiac dysfunction with age [15]. Studies show that patients with age-related liver diseases such as cirrhosis and fatty liver disease can develop electrophysiological cardiac abnormalities [16,17] and systolic [18] and diastolic [19] dysfunction. A range of hepatic mediators, such as extracellular vesicles (EVs), proteins, microRNAs, miR1, miR7, and miR-122, that are produced and secreted primarily or exclusively by the liver are believed to influence the cardiovascular system through endocrine mechanisms. Growing evidence underscores the significant role these liver-derived factors play in the development and progression of various

cardiovascular diseases, including atherosclerosis, coronary heart disease, thrombosis, myocardial infarction, heart failure, metabolic cardiomyopathy, arterial hypertension, and pulmonary hypertension [20]. However, the causal relationship between hepatic aging and heart disease has not been fully elucidated.

Cellular senescence is a stable and generally irreversible form of cell cycle arrest that occurs in response to a variety of stressors, including DNA damage, telomere shortening, and oxidative stress, and is a core hallmark of aging [21]. Senescent cells no longer divide but remain metabolically active and often acquire a SASP profile [22]. In this study, we developed an in vitro platform to model liver aging using HepG2 cells treated with hydrogen peroxide, a wellestablished method to induce oxidative stress for accelerated aging [23], in which senescent markers served as our primary indicator of the aged phenotype. The conditioned media from these aged liver cells were then used to treat human induced pluripotent stem cell-derived cardiomyocytes (iCMs), where we then assessed the in vitro 'paracrine' impact of the aged liver secretome on cardiac cell aging and/or dysfunction by measuring and confirming aged phenotypes using senescence, oxidative stress, lipofuscin accumulation, and p21 immunostaining assays. Here, we aimed to delineate the effect of liver-derived secretions on iCM health and aging. Our study offers new insights into the mechanistic underpinnings of liver-heart communication in aging and shows potential for therapeutic intervention which targets inter-organ signaling pathways.

2. Materials and methods

2.1. iPSC cell culture and maintenance

Human skin fibroblast-derived iPS cell line hiPS-K3 cells were kindly provided by Dr. Stephen Duncan (Medical College of Wisconsin). T-75 flasks were coated with a 1:100 (v/v) dilution of Geltrex™(ThermoFisher Scientific) in Dulbecco's Modified Eagle Medium (DMEM; Gibco) and incubated at 37 °C for 30 minutes. Fifteen minutes prior to coating, two 15 mL conical tubes were prepared: one containing 5 mL of mTeSR™Plus medium (StemCell Technologies) supplemented with a final concentration of 5 μM ROCK inhibitor (StemCell Technologies), and the other containing 10 mL mTeSR™Plus medium supplemented with a final concentration of 5 μM ROCK inhibitor. The 10 mL tube was pre-warmed to 37 °C. Human induced pluripotent stem cells (iPSCs; iPS-K3 cell line) were retrieved from liquid nitrogen storage and rapidly thawed in the water bath for 1 minute. The thawed cell suspension was immediately transferred to the 5 mL mTeSR™Plus/ROCK inhibitor solution and centrifuged at 300 $\times$ g for 5 minutes. Concurrently, the Geltrex™solution was aspirated from the pre-coated flask and aseptically dried. Nine milliliters of the pre-warmed 10 mL mTeSR™Plus medium were added to the flask. The pellet was gently resuspended in 1 mL of the remaining mTeSR™Plus medium and transferred to the prepared flask. Media was changed daily for 4 days or until cells reached approximately 70% confluency. Cells were subsequently passaged using ReLeSR™(StemCell Technologies) and expanded as required, with daily media changes maintained throughout. The iPSCs were seeded at a density of 5 $\times$ 10^5 cells per well onto Geltrex™-coated 24-well plates for differentiation experiments.

2.2. Cardiomyocyte differentiation from iPSCs

Cardiomyocyte differentiation was initiated when iPSCs cultured in Geltrex™-coated 24- well plates reached >90% confluency, following previously established protocols. All media components and supplements were freshly prepared on the day of use. From days 0 to 6, differentiation was carried out in cardiomyocyte differentiation medium without insulin (CM (-)), consisting of 500 mL RPMI 1640 (Gibco, 11875), 10 mL B-27 Supplement minus insulin (Gibco), and 5 mL penicillin-streptomycin (Pen/Strep; Sigma-Aldrich). On day 1 of differentiation the cells were treated with 10 μM CHIR 99021, and the media was replaced with standard CM (-) within 24 hours. On day four of differentiation, the cells were treated with CM (-) media supplemented with 5 μM IWP4. On the sixth day, standard CM (-) media was reintroduced. From day 7 onwards, a CM (+) medium was utilized, which consisted of 500 mL RPMI 1640, 10 mL B-27 Supplement with insulin (Gibco), and 5 mL Pen/Strep.

2.3. HepG2 culture and artificial aging

HepG2 cells (ATCC) were cultured in complete Dulbecco's Modified Eagle Medium (DMEM), prepared by supplementing DMEM (Gibco) with 10% fetal bovine serum (FBS; Invitrogen) and 1%

penicillin-streptomycin (Pen/Strep; ThermoFisher Scientific). Cells were retrieved from liquid nitrogen storage and thawed in a 37 °C water bath for 1 minute. The thawed suspension was transferred into 5 mL of pre-warmed complete DMEM and centrifuged at 200 × g for 5 minutes. The resulting cell pellet was resuspended in 1 mL of fresh medium and transferred into a T-75 flask containing 9 mL of complete DMEM. Cells were evenly distributed by gentle swirling and incubated at 37 °C with 5% CO_2. Media changes were performed every three days until cells reached the desired confluency. For subculturing, cells were rinsed with phosphatebuffered saline (PBS; Gibco) and detached using 0.05% trypsin-EDTA (Gibco). Following cell counting via hemocytometer, 1.5×10^5 cells were seeded per well in 24-well plates. After allowing 1–2 days for cellular adherence and acclimatization, oxidative stress treatments were initiated. Cells were exposed to hydrogen peroxide (H_2O_2) at various concentrations and durations to induce aging. The treatment groups were as follows (Table 1):

Table 1. Oxidative aging treatment plan

Treatment Duration	H_2O_2 Concentration (μM)
21 days	25, 50
15 days	50, 100
7 days	200, 300

Corresponding untreated control groups were maintained for each time point. Media containing the appropriate H_2O_2 concentrations were refreshed every two days. At the end of each aging period, conditioned HepG2 media was collected, labeled, and stored at -20 °C for downstream analyses of liver secretome effects. Cells used for phenotypic aging characterization were fixed at the end of treatment.

2.4. Oxidative stress detection

Oxidative stress in monolayer cultures was evaluated using the CellROX™Green Reagent (Thermo Fisher Scientific), a fluorogenic probe that emits fluorescence upon oxidation, to detect general levels of reactive oxygen species (ROS). A 5 μM working solution was prepared by diluting the 2.5 mM DMSO-stabilized stock into complete DMEM. At the conclusion of the 7-day and 15-day oxidative stress treatments, the existing culture media were removed and replaced with the CellROX working solution. Cells were incubated at 37 °C for 30 minutes, followed by three PBS washes. Nuclear staining was performed using a 1 μg/mL Hoechst solution, and a final PBS wash was completed prior to imaging. Samples were imaged within two hours using a fluorescence microscope at excitation/emission wavelengths of 485/520 nm. For each sample, a minimum of five images per well were captured. Quantitative analysis of oxidative stress was performed using ImageJ by measuring the mean gray value intensity of individual cells.

2.5. Treatment of iCMs with aged liver secretions

After the iCM differentiation period, aged liver-conditioned media were applied to evaluate the impact of hepatic secretions on cardiac cell aging. iCM media were removed and replaced with varying dilutions of aged liver media as follows: (1) undiluted aged liver media (DMEM), (2) a 1:1 dilution of aged liver media with iCM media, and (3) a 1:3 dilution of aged liver media with iCM media. To control for potential effects of liver media unrelated to aging, parallel treatments using regular (non-aged) liver media were performed with identical dilution ratios. An additional control group consisted of iCM media alone. All treatments were applied for a duration of three days. Following the treatment period, iCMs were fixed in 4% paraformaldehyde and processed for the assessment of aging-associated markers.

2.6. Lipofuscin Granule Staining

Following fixation with 4% paraformaldehyde, HepG2 cells and iPSC-derived cardiomyocytes (iCMs) were stained using Sudan Black B (SBB) to assess lipofuscin accumulation. The SBB staining solution was prepared by dissolving 0.7 g of SBB powder (Sigma- Aldrich) in 100 mL of 70% ethanol. The mixture was covered with Parafilm and stirred overnight at low speed using a magnetic stir bar. The resulting solution was filtered through 11 cm Whatman circle filter paper to remove any undissolved particles. Prior to staining, cells were incubated in 70% ethanol for 2 minutes. SBB stain was then applied to each well and incubated for 2–5

minutes, followed by three washes with 50% ethanol or until the wash ran clear. Images were acquired using a Nikon Eclipse Ti-U inverted microscope (Bright Field mode) equipped with NIS-Elements imaging software. Five representative images were captured per well. Quantitative analysis of staining intensity was performed using ImageJ software.

2.7. Immunofluorescence Staining for p21 Expression

HepG2 cells and iPSC-derived cardiomyocytes (iCMs) were stained for p21 expression using a monoclonal anti-p21 antibody (Invitrogen, Thermo Fisher Scientific) and the Alexa Fluor™488 Goat Anti-Rabbit SFX Kit, following standard immunocytochemistry procedures. All media and reagents were prepared before initiating the staining protocol. Cells were first permeabilized with 0.2% Triton X-100 in PBS for 15 minutes at room temperature, followed by three washes with 500 μL of PBS. Non-specific binding was blocked by incubating the cells in 200 μL of 10% goat serum for 1 hour at room temperature. After removal of the blocking serum, cells were incubated overnight at 4°C with 200 μL of 10% goat serum containing the primary antibody (1:300 dilution). Plates were sealed with Parafilm to prevent evaporation during incubation. The primary antibody solution was removed after 24 hours, and cells were washed five times with 500 μL of PBS at 5-minute intervals (subsequent steps were performed under low-light conditions). Cells were then incubated for 2–4 hours at 4°C with 200 μL of 10% goat serum containing the secondary antibody (1:500 dilution), protected from light with aluminum foil. Following secondary antibody incubation, cells were washed five times with PBS. The first wash included Hoechst 33342 nuclear stain (1:1000 dilution in PBS), while the remaining four washes removed excess stain and background fluorescence. Fluorescent imaging was conducted using a Nikon Eclipse Ti-U microscope equipped with NIS-Elements software. Hoechst and Alexa Fluor 488 channels were used to visualize nuclei (blue) and p21 (green), respectively. Five images were acquired per channel per well (ten images total per well). Quantitative analysis of nuclear and p21- positive cell counts was performed using ImageJ software.

2.8. Senescence-associated β-galactosidase staining

Senescence in HepG2 cells and iPSC-derived cardiomyocytes (iCMs) was assessed using the Senescence Cells Histochemical Staining Kit (Millipore Sigma, Catalog # CS0030), following the manufacturer's protocol. Cells were fixed with 4% paraformaldehyde, the provided staining solution was applied directly to the wells of HepG2 and iCM plates, and plates were sealed with Parafilm. Samples were incubated overnight at 37 °C in a non-CO_2 incubator. After incubation, the staining solution was removed and replaced with PBS. Brightfield images were acquired using the Nikon Eclipse Ti-U microscope with Infinity Capture software, under standard light settings and without color filters. Five images were captured per well. Quantitative analysis of senescencepositive cells was performed using ImageJ software.

2.9. Statistical analysis

All data were analyzed using Microsoft Excel Data Analysis Toolpak (Version 16.77.1). To assess significance between control and treatment groups, a two-tailed paired t-test was performed. A one-way ANOVA with post hoc analysis was used to evaluate differences within treatment groups. Statistical significance was defined as $P < 0.05$ for all tests.

3. Results

3.1. Hydrogen peroxide treatment induces aged phenotype in HepG2 cells

A comprehensive analysis of our artificial aging process was conducted by examining the percentage of lipofuscin granule-positive (LPF^+) cells, p21 expression-positive ($p21^+$) cells, and senescent cells in HepG2 cultures (Supplementary Figure 1) upon several different H_2O_2 treatments. Treated HepG2s showed significantly increased % LPF^+ cells (Supplementary Figure 1A) under the 7-day 200 μM treatment group (24.5 $\pm$ 15.7%) compared to untreated controls (9.8 $\pm$ 1.7%, $p < 0.01$). A significant difference between 7-day 200 μM and 21-day 50 μM treatment groups was also shown ($p < 0.001$). The efficacy of treatment is unclear from p21 immunostaining results (Supplementary Figure 1B). However, a significant difference in % $p21^+$ HepG2s

was observed under the 15-day treatment group, where the p21$^+$ HepG2 population was 61.1 $\pm$ 4.7% under 100 μM and 36.4 $\pm$ 7.2% under 50 μM treatment ($p < 0.02$).

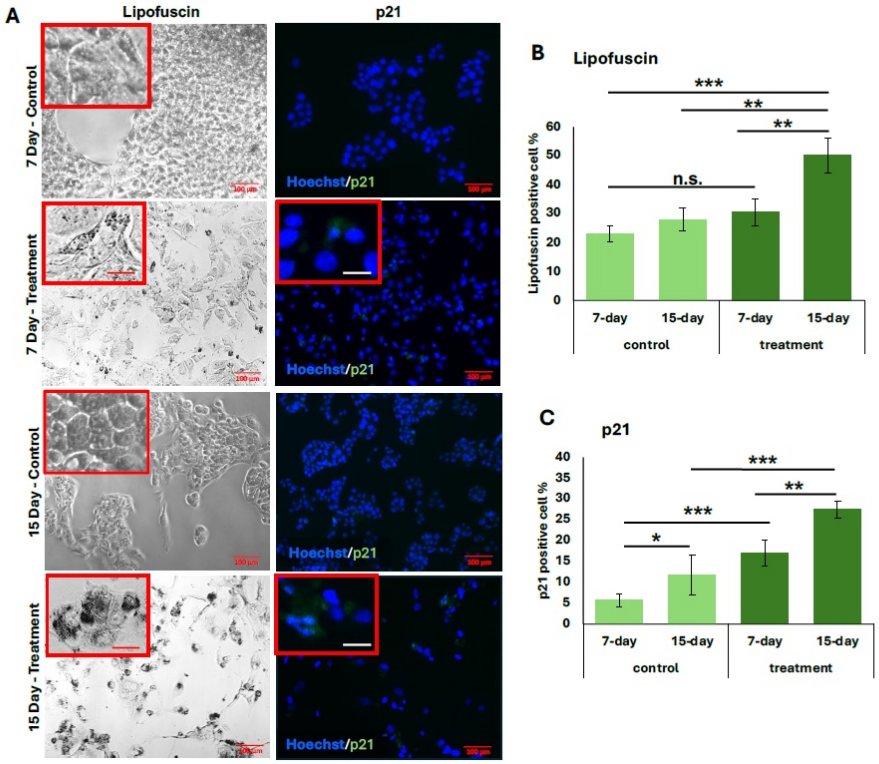

Figure 1. H_2O_2 treatment leads to increased p21 expressing cells and cellular waste accumulation in HepG2s. (A) Bright-field and fluorescence images showing levels of lipofuscin accumulation (left) and p21 expression (right), respectively, in liver cells receiving 7-day (200 mM H_2O_2) and 15-day (100 mM H_2O_2) treatment and respective controls. (B) HepG2 cell percentage that show lipofuscin accumulation. (C) Percent p21 expressing HepG2 cells. (* represents statistical significance with $p < 0.05$, ** represents statistical significance with $p < 0.01$, *** represents statistical significance with $p < 0.001$, and n.s. represents no statistical significance) (Scale bars = 100 mm, inset scale bars = 30 mm) ($n = 5$)

In addition, 7-day 200 μM treatment (Supplementary Figure 1C) showed an increase in % senescence (9.9 $\pm$ 1.2%) in comparison to the untreated control group (0.8 $\pm$ 0.7%, $p < 0.02$). In this case, the 15-day 100 μM treatment (6.1 $\pm$ 1.3%) was less effective than the 7-day 200 μM treatment in inducing senescence.

3.2. Select hydrogen peroxide treatments induce an increase in LPF$^+$ and p21$^+$ HepG2 cells

To validate that aged liver secretions were appropriately derived from senescent HepG2 cells, we confirmed the presence of aging markers in liver cultures prior to media transfer to iCMs. This step was essential to eliminate confounding variables that could misrepresent the downstream effects on iCMs. Based on previous findings, 7-day 200 μM and 15-day 100 μM conditions exhibited their potential for effective artificial induced aging of HepG2 cells. Consequently, experimentation was refined henceforth to prioritize these concentrations.

As shown in Figure 1, HepG2 cells treated with hydrogen peroxide for 7 and 15 days exhibited significantly increased lipofuscin granule accumulation and p21 expression. From quantification, the 15-day treatment group demonstrated the highest proportion of LPF$^+$ cells (50.2 $\pm$ 0.04%), with strong statistical significance compared to both the 7-day treatment group ($p < 0.001$) and untreated controls ($p < 0.001$ and $p < 0.002$, respectively) (Figure 1B).

Similarly, p21 expression was significantly elevated in both treatment groups relative to their controls (Figure 1C), with the 15-day group showing a greater percentage of p21$^+$ cells (27.5 $\pm$ 0.06%) compared to the 7-day group (15.5 $\pm$ 0.01%) ($p < 0.008$). The proportion of senescent cells also increased following both treatment durations, and representative general oxidative stress levels are indicated in green for

comparison (Figure 2A). The 15-day H_2O_2 treatment group exhibited the highest percentage of senescent cells (34.0 $\pm$ 0.02%), showing strong statistical significance compared to the 7-day treatment group (18.8 $\pm$ 0.03%, $p < 0.001$) and to the corresponding untreated controls ($p < 0.001$) (Figure 2B). Similarly, cells subjected to the 15-day 100 μM H_2O_2 treatment showed the highest levels of oxidative stress, as measured by MFI (5.8 $\pm$ 3.0). This was significantly greater than the MFI observed in the 7-day 100 μM treatment group (1.5 $\pm$ 0.59, $p < 0.0001$). Furthermore, oxidative stress in the 15-day treatment group was elevated compared to its untreated control ($p < 0.001$) (Figure 2C).

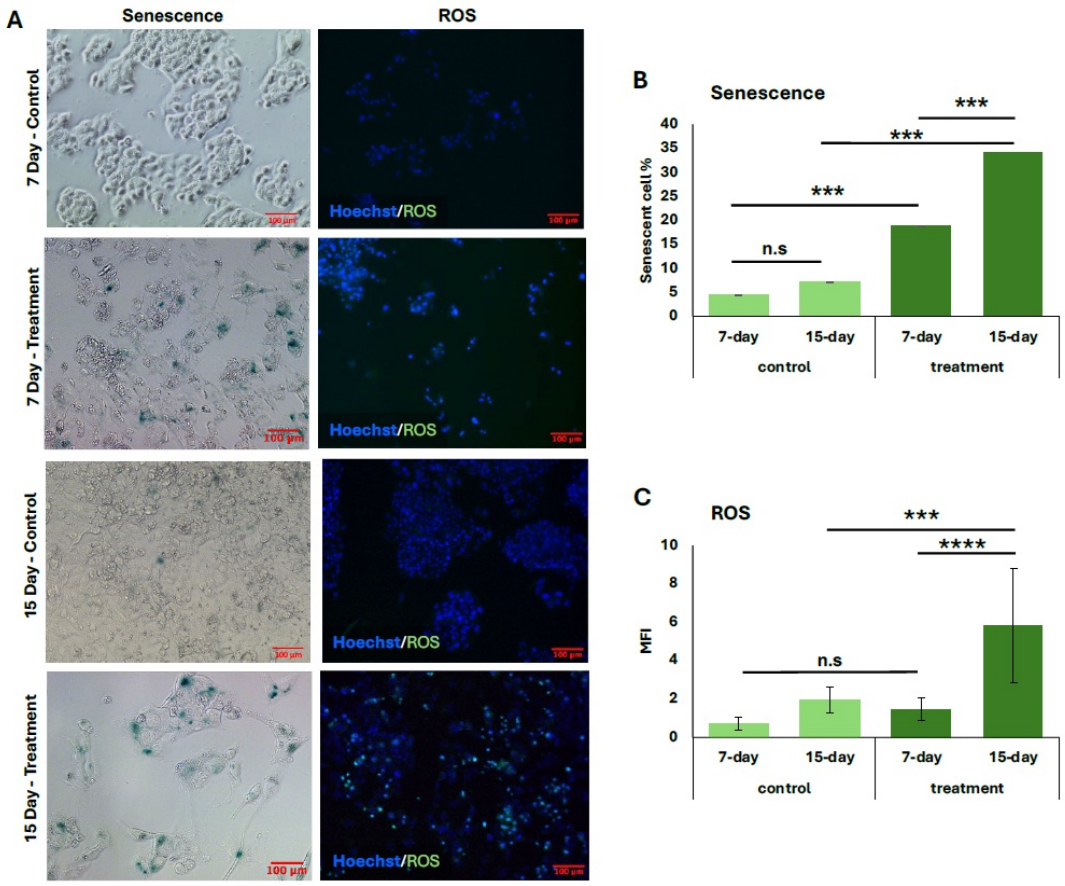

Figure 2. Cellular senescence and ROS accumulation significantly increases with the aging treatment in HepG2s. (A) Bright-field and fluorescence images showing cellular senescence (right) and ROS accumulation in liver cells receiving 7-day (200 mM H_2O_2) and 15-day (100 mM H_2O_2) treatment as well as their respective controls. (B) Senescent HepG2 cell percentage. (C) Quantified oxidative stress levels as mean fluorescent intensity (MFI) representing relative ROS accumulation in HepG2 cells. MFI was determined by subtracting background mean gray value (MGV) from fluorescent MGV was plotted. (*** represents statistical significance with $p < 0.001$, **** represents statistical significance with $p < 0.0001$, and n.s. represents no statistical significance) (Scale bars = 100 mm)

3.3. iCM senescence/waste accumulation not influenced by culture in different control media

Fresh DMEM and untreated liver-conditioned media were applied to untreated iCMs as control conditions to evaluate the potential effects of solely liver media composition or secretome on aging-related markers, including senescence and lipofuscin waste accumulation (Figure 3). Results were compared to iCMs maintained in native media. No statistically significant differences were observed among the control groups in the % LPF^+ cells (Figure 3A). Although a significant increase was observed in senescent cell percentage when iCMs received untreated liver-conditioned media, this difference was nearing no significance (Figure 3B).

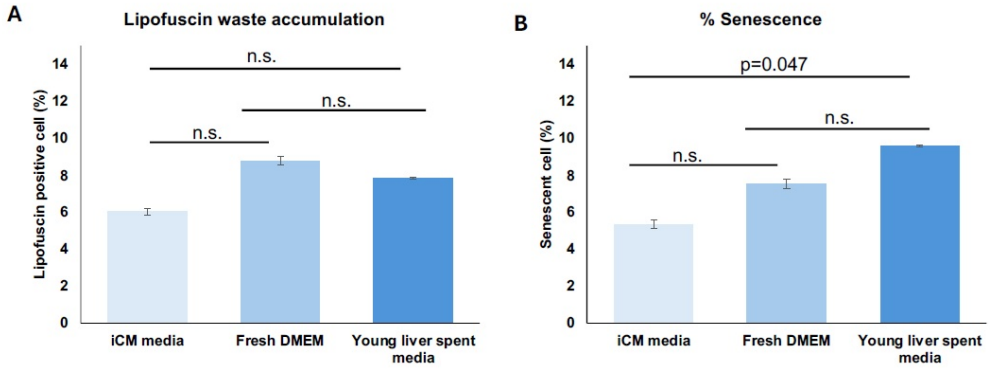

Figure 3. iCM senescence or waste accumulation are not affected by culture in different control media. (A) Percent lipofuscin waste accumulation positive and (B) senescent iCMs cultured for 7 days with different control media. (n.s. represents no statistical significance) (n=3)

3.4. Aging in iCMs is induced by aged liver secretome and is dose-dependent

Varying dilutions of aged liver-conditioned media with standard iCM media were tested to identify an optimal treatment condition that preserved iCM viability while still enabling the assessment of aging-associated effects. Specifically, iCMs were treated with undiluted aged liver media (DMEM only), as well as 1:1 and 1:3 dilutions of aged liver media with iCM media (Supplementary Figures 2 and 3). A significant dilution-dependent uniform reduction in lipofuscin accumulation was observed (Supplementary Figure 2A, 3A), and the effect was more pronounced for 15-day treatments ($p < 0.001$). For both the 7-day and 15-day aged liver media treatments, the highest % LPF$^+$ cells occurred under the undiluted condition, with progressively lower accumulation levels for 1:1 and 1:3 dilutions. The p21 expression parameter followed a similar dilution-dependent trend in iCMs (Supplementary Figure 2B, 3B). While % p21$^+$ cells decreased with increasing dilution of aged liver media, no statistically significant differences were detected between the 7-day and 15-day treatment groups across the DMEM-only, 1:1, or 1:3 dilutions. Regarding senescence (Supplementary Figure 2C, 3C), iCMs exhibited a modest reduction in senescent cell proportions when treated with 1:3 dilution of aged liver media. Interestingly, a substantial peak in senescence was observed under the 1:1 dilution condition in both treatment groups, reaching 40.3 $\pm$ 0.02% for the 7-day group and 56.0 $\pm$ 0.03% for the 15-day group.

We then performed further characterization of undiluted aged liver-conditioned media to evaluate its ability to induce aged phenotypes in iCMs, focusing on waste accumulation (LPF$^+$), p21 expression, and senescence markers. A significant increase in the percentage of LPF$^+$ iCMs was observed in all groups treated with aged liver spent media, as shown in Figure 4A. Both 7-day and 15-day treatment conditions resulted in significantly higher LPF$^+$ cell populations compared to controls ($p < 0.01$). Notably, iCMs exposed to 15-day aged liver media exhibited greater LPF$^+$ accumulation compared to those treated with 7-day aged media ($p < 0.01$) (Figure 4B). Consistent with waste accumulation data, p21 expression was also elevated in iCMs treated with aged liver spent media compared to young spent media. Both the 7-day and 15-day treatment groups using aged spent media yielded significantly increased populations of p21$^+$ cells, visualized as fluorescent green in Figure 5A. Quantification revealed a statistically significant upregulation in p21 expression for both treatment durations compared to young spent media, with the 15-day treatment group demonstrating a more prominent effect (Figure 5B) ($p < 0.01$, 7-day; $p < 0.001$, 15-day). Lastly, senescence data mirrors our findings regarding p21 expression. The increased proportion of stained cells (bluish green) indicates a discernible qualitative enhancement in senescent cell % from SA-β-Gal activity (Figure 6A). Similarly, aged liver spent media from each treatment duration group exhibited a more pronounced impact on iCMs compared to young spent media controls ($p < 0.01$, 7-day; $p < 0.001$, 15-day) (Figure 6B).

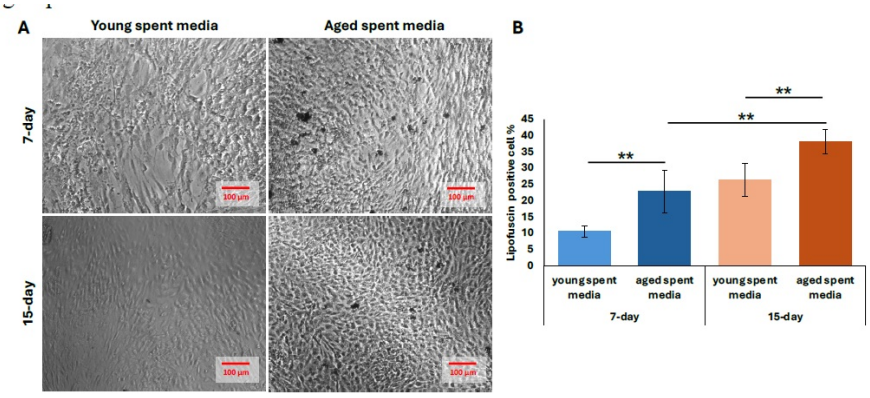

Figure 4. Significant increase in cellular waste accumulation in iCMs is observed upon treatment with aged spent liver media. (A) Bright-field images showing lipofuscin waste accumulation, and percent lipofuscin waste accumulation positive iCMs treated with young or aged liver spent media. (** represents statistical significance with $p < 0.01$, *** represents statistical significance with $p < 0.001$) (Scale bars = 100 mm) ($n = 5$)

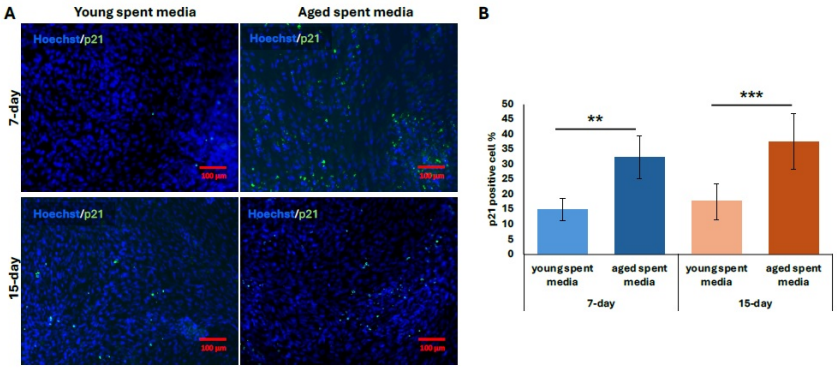

Figure 5. Percentage of p21 expressing iCMs increases upon exposure to aged liver spent media. (A) Immunofluorescent images (nuclei, blue; p21, green) and (B) percentage of p21 positive iCMs treated with young or aged liver spent media. (** represents statistical significance with p<0.01, *** represents statistical significance with p<0.001) (Scale bars= 100 mm) (n=5)

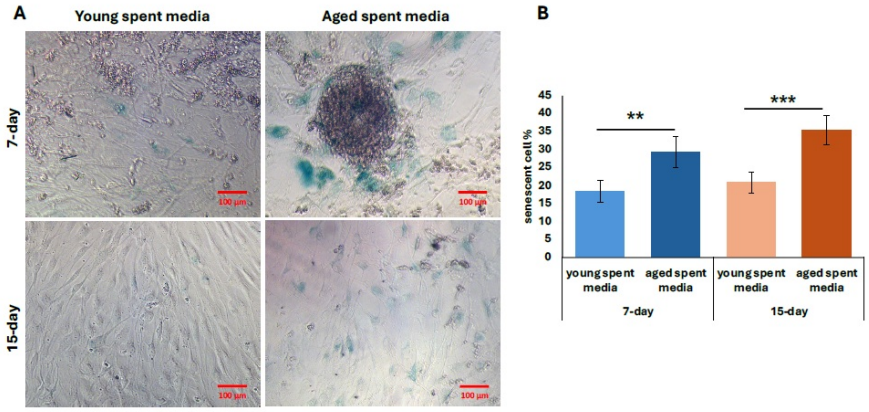

Figure 6. Incubation with aged liver spent media leads to increased senescence in iCMs. (A) Brightfield images of senescence and (B) percent senescence in iCMs treated with young or aged liver spent media. (** represents statistical significance with p<0.01, *** represents statistical significance with p<0.001) (Scale bars= 100 mm) (n=5)

4. Discussion

The liver and heart maintain a complex bidirectional relationship, with dysfunction in one organ significantly impacting the other. This interaction is most commonly discussed under the umbrella of cardiohepatic syndromes (CHS), which include heart failure-induced liver injury and liver disease-related cardiac dysfunction [24,25]. However, neither this relationship nor the significance of CHS is fully understood, particularly regarding aging-related diseases. In this study, we aimed to develop and validate an in vitro model of oxidative liver aging and investigate its paracrine effects on iCMs. Through hydrogen peroxide-induced aging of HepG2 cells, we observed hallmark senescence features including increased lipofuscin accumulation and elevated p21 expression, heightened β-galactosidase activity, and oxidative stress. Our findings from aging characterizations highlighted the association of lipofuscin granule accumulation with oxidative damage and aging phenotypes. Lipofuscin accumulation is a well-recognized hallmark of aging and is intricately linked to oxidative stress and impaired cellular clearance mechanisms [26,27]. Composed primarily of oxidized proteins, lipids, carbohydrates, and metal residues, lipofuscin granules are autofluorescent, undegradable by lysosomal enzymes, and progressively accumulate within post-mitotic and slowly dividing cells, which include both hepatocytes and cardiomyocytes [28,29]. From our preliminary aging experiment, HepG2 cells treated with hydrogen peroxide yielded a higher LPF^+ cell population than the untreated samples, suggesting an accumulation of lipofuscin granules consistent with oxidative damage and aging phenotypes. A customized platform developed by Gaspar et al. [30] demonstrated the efficacy of hydrogen peroxide treatment combined with Fenton chemistry in promoting lipofuscin generation. Their protocol utilized a 10 μM hydrogen peroxide concentration in the cell culture medium with media changes every 48 hours for 10 days to create sustained oxidative conditions. Flow cytometry analysis revealed increased autofluorescence intensity indicative of substantial lipofuscin accumulation, achieved without the need for a 40% hyperoxic chamber. These findings corroborate the efficacy of peroxide-based oxidative induction models, and while more extreme, support our data obtained from stronger peroxide concentrations without ferrous ion enhancement.

Cellular senescence is induced by p21/p53 pathways, primarily mediating cell cycle arrest in response to stress signals. p21Cip1/Waf1 is a cyclin-dependent kinase inhibitor (CDKI) encoded by the CDKN1A gene and is a downstream effector of the p53 tumor suppressor pathway. Upon activation, p21 binds and inhibits cyclin-CDK complexes effectively halting the cell cycle in G1 or S phase [31]. Additionally, during cellular (oxidative) stress, p53 is stabilized and transcriptionally upregulates p21, leading to a durable cell cycle arrest [32]. A study conducted by Zhou et al. [33] incubated isolated cartilage end plate (CEP) cells with 150 μM hydrogen peroxide to activate the p21/p53 pathway through oxidative stress, and their p21 expression and senescence data were comparable to those within our study. Relative p21 expression was significantly increased by 7-fold from H2O2 treatment alone. In addition, the inhibition of p53 using Pifithrin-α was found to prevent oxidative stress-induced senescence. The percentage of SA-β-Gal^+ cells was also found to be markedly increased (20% vs 70%, $p < 0.05$). Another study reported successful induction of senescence in normal AML12 hepatic cells [34]. Likewise, a repetitive 750 μM hydrogen peroxide treatment was applied for 5 days and increased mRNA expression of CDKN1A/p21 marker genes was observed compared to control untreated AML12 cells. Moreover, SA-β-Gal^+ cells were increased approximately 8-fold in treated cells [34], confirming the induction of premature senescence in hepatocytes through repeated hydrogen peroxide exposure, as expressed in our methods.

Conditioned media from confirmed aged HepG2 cells were introduced to iCMs, and the strongest effect was observed in undiluted dosages. The aged liver secretome likely contains a variety of pro-aging factors capable of influencing cardiomyocyte behavior and function. A primary component of this secretome is the SASP, which includes inflammatory cytokines such as IL-6, IL-1β, TNF-α, IL-8, and TGF-β, as well as matrix-degrading enzymes like MMPs. These factors can likely promote cellular senescence, fibrosis, and extracellular matrix remodeling in heart cells, mirroring pathologies observed in aged cardiac tissue [35,36]. In addition, the secretome may include reactive oxygen species (ROS) and lipofuscin-like aggregates, which act as damageassociated molecular patterns (DAMPs) [37]. These components have the potential to elevate oxidative stress in iCMs, triggering stress response pathways and promoting cellular dysfunction. EVs, particularly exosomes released by senescent liver cells, further contribute to the pro-aging effects by transporting regulatory molecules such as miR-34a, miR-21 and miR-217 (increased due to oxidative stress). These miRNAs can modify gene expression in recipient iCMs, impair mitochondrial function, and

drive senescence-like phenotypes [38–41]. Several studies have also confirmed that such vesicles carrying miRNAs (among other molecules) are capable of eliciting systemic aging effects [42–44]. Interestingly, while other markers like lipofuscin and p21 followed a more intuitive dose-dependent pattern, SA-β-Gal activity was highly favored in 1:1 dilution of conditioned/iCM media, as evidenced by our data. The activity of β-Galactosidase is typically measured at a pH of 6 [45]. It is plausible that the constituent liver and iCM media from 1:1 ratios were of dissimilar pH levels, which may have created the optimal pH range (6) for measurement from their combination.

Our study demonstrates that artificially aged liver cells secrete factors capable of inducing aging-like phenotypes in cardiomyocyte cultures. Using a hydrogen peroxide-based protocol, we successfully modeled liver aging, characterized by elevated lipofuscin accumulation, increased p21 expression, heightened oxidative stress, and cellular senescence. Upon transferring aged liver secretome to iCMs, we observed consistent upregulation of these aging markers, supporting the hypothesis that the aging liver can contribute to cardiac aging via secretory factors. These findings showcase the influential role of the liver secretome in aging, thus targeting inter-organ signaling shows promise as an effective therapeutic strategy in age-related cardiac dysfunction. Future studies for identifying these secreted factors and determining the key factors that drive this communication and spread of aging will provide important insight to development of novel therapeutic targets.

References

[1] López-Otín, C., Blasco, M. A., Partridge, L., Serrano, M., & Kroemer, G. (2013). The Hallmarks of Aging. *Cell*, *153*(6), 1194–1217.

[2] Guo, J., Huang, X., Dou, L., Yan, M., Shen, T., Tang, W., & Li, J. (2022). Aging and agingrelated diseases: From molecular mechanisms to interventions and treatments. *Signal Transduction and Targeted Therapy*, *7*(1), 391.

[3] Tokizane, K., & Imai, S. (n.d.). Inter-organ communication is a critical machinery to regulate metabolism and aging. *Trends in Endocrinology & Metabolism*, *36*(8), 756-766.

[4] Tian, Y. E., Cropley, V., Maier, A. B., Lautenschlager, N. T., Breakspear, M., & Zalesky, A. (2023). Heterogeneous aging across multiple organ systems and prediction of chronic disease and mortality. *Nature Medicine*, *29*(5), 1221–1231.

[5] Rai, M., Coleman, Z., Curley, M., Nityanandam, A., Platt, A., Robles-Murguia, M., Jiao, J., Finkelstein, D., Wang, Y.-D., Xu, B., Fan, Y., & Demontis, F. (2021). Proteasome stress in skeletal muscle mounts a long-range protective response that delays retinal and brain aging. *Cell Metabolism*, *33*(6), 1137-1154.

[6] Tokizane, K., Brace, C. S., & Imai, S. (2024). DMHPpp1r17 neurons regulate aging and lifespan in mice through hypothalamic-adipose inter-tissue communication. *Cell Metabolism*, *36*(2), 377-392.

[7] Berasain, C., Arechederra, M., Argemí, J., Fernández-Barrena, M. G., & Avila, M. A. (2023). Loss of liver function in chronic liver disease: An identity crisis. *Journal of Hepatology*, *78*(2), 401–414.

[8] Higashi, T., Friedman, S. L., & Hoshida, Y. (2017). Hepatic stellate cells as key target in liver fibrosis. *Fibroblasts and Extracellular Matrix: Targeting and Therapeutic Tools in Fibrosis and Cancer*, *121*, 27–42.

[9] Berumen, J., Baglieri, J., Kisseleva, T., & Mekeel, K. (2021). LIVER FIBROSIS: Pathophysiology and Clinical Implications. *WIREs Mechanisms of Disease*, *13*(1), e1499.

[10] Kim, H., Kisseleva, T., & Brenner, D. A. (2015). Aging and liver disease. *Current Opinion in Gastroenterology*, *31*(3), 184–191.

[11] Bárcena, B., Salamanca, A., Pintado, C., Mazuecos, L., Villar, M., Moltó, E., Bonzón- Kulichenko, E., Vázquez, J., Andrés, A., & Gallardo, N. (2021). Aging Induces Hepatic Oxidative Stress and Nuclear Proteomic Remodeling in Liver from Wistar Rats. *Antioxidants*, *10*(10), 1535.

[12] Gong, J., Tu, W., Liu, J., & Tian, D. (2023). Hepatocytes: A key role in liver inflammation. *Frontiers in Immunology*, *13*, 1083780.

[13] Huang, Y., Yang, X., Meng, Y., Shao, C., Liao, J., Li, F., Li, R., Jing, Y., & Huang, A. (2021). The hepatic senescence-associated secretory phenotype promotes hepatocarcinogenesis through Bcl3-dependent activation of macrophages. *Cell & Bioscience*, *11*(1), 173.

[14] Szabo, G., & Momen-Heravi, F. (2017). Extracellular vesicles in liver disease and potential as biomarkers and therapeutic targets. *Nature Reviews Gastroenterology & Hepatology*, *14*(8), 455–466.

[15] Oishi, Y., & Manabe, I. (2020). Organ System Crosstalk in Cardiometabolic Disease in the Age of Multimorbidity. *Frontiers in Cardiovascular Medicine*, *7*, 64.

[16] Genovesi, S., Prata Pizzala, D. M., Pozzi, M., Ratti, L., Milanese, M., Pieruzzi, F., Vincenti, A., Stella, A., Mancia, G., & Stramba-Badiale, M. (2009). QT interval prolongation and decreased heart rate variability in cirrhotic patients:

Relevance of hepatic venous pressure gradient and serum calcium. *Clinical Science (London, England: 1979), 116*(12), 851–859.

[17] Kim, S. M., George, B., Alcivar-Franco, D., Campbell, C. L., Charnigo, R., Delisle, B., Hundley, J., Darrat, Y., Morales, G., Elayi, S.-C., & Bailey, A. L. (2017). QT prolongation is associated with increased mortality in end stage liver disease. World Journal of *Cardiology, 9*(4), 347–354.

[18] Ridjab, D. A., Ivan, I., Budiman, F., & Tenggara, R. (2022). Evaluation of subclinical ventricular systolic dysfunction assessed using global longitudinal strain in liver cirrhosis: A systematic review, meta-analysis, and meta-regression. *PLOS ONE, 17*(6), e0269691.

[19] Liu, Y., Meng, F., Ma, J., Zhang, W., Yu, J., Zhou, Y., Zuo, W., Yan, Z., Pan, C., & Luo, J. (2023). Diastolic Dysfunction in Cirrhotic Cardiomyopathy: A Prospective Observational Cohort Study on Short-Term Outcomes in Cirrhotic Patients Undergoing TIPS [Preprint]. In Review. https://doi.org/10.21203/rs.3.rs-2968905/v1

[20] Liu, X., Shao, Y., Han, L., Zhang, R., & Chen, J. (2023). Emerging Evidence Linking the Liver to the Cardiovascular System: Liver-derived Secretory Factors. *Journal of Clinical and Translational Hepatology, 11*(5), 1246–1255.

[21] McHugh, D., & Gil, J. (2018). Senescence and aging: Causes, consequences, and therapeutic avenues. *Journal of Cell Biology, 217*(1), 65–77.

[22] Coppé, J.-P., Desprez, P.-Y., Krtolica, A., & Campisi, J. (2010). The Senescence-Associated Secretory Phenotype: The Dark Side of Tumor Suppression. *Annual Review of Pathology: Mechanisms of Disease, 5*(1), 99–118.

[23] Acun, A., Nguyen, T. D., & Zorlutuna, P. (2019). In vitro aged, hiPSC-origin engineered heart tissue models with age-dependent functional deterioration to study myocardial infarction. *Acta Biomaterialia, 94*, 372–391.

[24] Laribi, S., & Mebazaa, A. (2014). Cardiohepatic syndrome: Liver injury in decompensated heart failure. *Current Heart Failure Reports, 11*(3), 236–240.

[25] Stolz, L., Orban, M., Karam, N., Lubos, E., Wild, M., Weckbach, L., ... & Hausleiter, J. (2023). Cardio-hepatic syndrome in patients undergoing mitral valve transcatheter edge-to-edge repair. *European Journal of Heart Failure, 25*(6), 872-884.

[26] Baldensperger, T., Jung, T., Heinze, T., Schwerdtle, T., Höhn, A., & Grune, T. (2024). The age pigment lipofuscin causes oxidative stress, lysosomal dysfunction, and pyroptotic cell death. *Free Radical Biology and Medicine, 225*, 871–880.

[27] Moreno-García, A., Kun, A., Calero, O., Medina, M., & Calero, M. (2018). An Overview of the Role of Lipofuscin in Age-Related Neurodegeneration. *Frontiers in Neuroscience, 12*, 464.

[28] Terman, A., Kurz, T., Navratil, M., Arriaga, E. A., & Brunk, U. T. (2010). Mitochondrial Turnover and Aging of Long-Lived Postmitotic Cells: The Mitochondrial–Lysosomal Axis Theory of Aging. *Antioxidants & Redox Signaling, 12*(4), 503–535.

[29] Tonolli, P. N., Martins, W. K., Junqueira, H. C., Silva, M. N., Severino, D., Santacruz-Perez, C., Watanabe, I., & Baptista, M. S. (2020). Lipofuscin in keratinocytes: Production, properties, and consequences of the photosensitization with visible light. *Free Radical Biology & Medicine, 160*, 277–292.

[30] Gaspar, J., Mathieu, J., & Alvarez, P. (2016). A rapid platform to generate lipofuscin and screen therapeutic drugs for efficacy in lipofuscin removal. *Materials, Methods and Technologies, 10*, 1-9.

[31] Childs, B. G., Durik, M., Baker, D. J., & van Deursen, J. M. (2015). Cellular senescence in aging and age-related disease: From mechanisms to therapy. *Nature Medicine, 21*(12), 1424–1435.

[32] Muñoz-Espín, D., & Serrano, M. (2014). Cellular senescence: From physiology to pathology. *Nature Reviews Molecular Cell Biology, 15*(7), 482–496.

[33] Zhou, N., Lin, X., Dong, W., Huang, W., Jiang, W., Lin, L., ... & Hu, Z. (2016). SIRT1 alleviates senescence of degenerative human intervertebral disc cartilage endo-plate cells via the p53/p21 pathway. *Scientific Reports, 6*(1), 22628.

[34] Singh, B. K., Tripathi, M., Sandireddy, R., Tikno, K., Zhou, J., & Yen, P. M. (2020). Decreased autophagy and fuel switching occur in a senescent hepatic cell model system. *Aging (Albany NY), 12*(14), 13958–13978.

[35] Ogrodnik, M., Miwa, S., Tchkonia, T., Tiniakos, D., Wilson, C. L., Lahat, A., ... & Jurk, D. (2017). Cellular senescence drives age-dependent hepatic steatosis. *Nature Communications, 8*(1), 15691.

[36] Freund, A., Orjalo, A. V., Desprez, P.-Y., & Campisi, J. (2010). Inflammatory Networks during Cellular Senescence: Causes and Consequences. *Trends in Molecular Medicine, 16*(5), 238–246.

[37] Ma, M., Jiang, W., & Zhou, R. (2024). DAMPs and DAMP-sensing receptors in inflammation and diseases. *Immunity, 57*(4), 752–771.

[38] Cui, H., Ge, J., Xie, N., Banerjee, S., Zhou, Y., Antony, V. B., Thannickal, V. J., & Liu, G. (2017). miR-34a Inhibits Lung Fibrosis by Inducing Lung Fibroblast Senescence. *American Journal of Respiratory Cell and Molecular Biology, 56*(2), 168–178.

[39] Takasugi, M. (2018). Emerging roles of extracellular vesicles in cellular senescence and aging. *Aging Cell, 17*(2), e12734.

[40] Mensà, E., Guescini, M., Giuliani, A., Bacalini, M. G., Ramini, D., Corleone, G., ... & Olivieri, F. (2020). Small extracellular vesicles deliver miR-21 and miR-217 as pro-senescence effectors to endothelial cells. *Journal of Extracellular Vesicles, 9*(1), 1725285.

[41] van Niel, G., D'Angelo, G., & Raposo, G. (2018). Shedding light on the cell biology of extracellular vesicles. *Nature Reviews Molecular Cell Biology, 19*(4), 213–228.

[42] Fulzele, S., Mendhe, B., Khayrullin, A., Johnson, M., Kaiser, H., Liu, Y., Isales, C. M., & Hamrick, M. W. (2019). Muscle-derived miR-34a increases with age in circulating extracellular vesicles and induces senescence of bone marrow stem cells. *Aging, 11*(6), 1791–1803.

[43] Alibhai, F. J., Lim, F., Yeganeh, A., DiStefano, P. V., Binesh-Marvasti, T., Belfiore, A., ... & Li, R. K. (2020). Cellular senescence contributes to age-dependent changes in circulating extracellular vesicle cargo and function. *Aging Cell, 19*(3), e13103.

[44] Law, B. A., Liao, X., Moore, K. S., Southard, A., Roddy, P., Ji, R., Szulc, Z., Bielawska, A., Schulze, P. C., & Cowart, L. A. (2018). Lipotoxic very-long-chain ceramides cause mitochondrial dysfunction, oxidative stress, and cell death in cardiomyocytes. *The FASEB Journal, 32*(3), 1403–1416.

[45] Valieva, Y., Ivanova, E., Fayzullin, A., Kurkov, A., & Igrunkova, A. (2022). Senescence- Associated β-Galactosidase Detection in Pathology. *Diagnostics, 12*(10), 2309.